REPORT DOCUMENTATION PAGE

Form Approved
OMB No. 0704-0188

1. REPORT DATE *(DD-MM-YYYY)*	2. REPORT TYPE	3. DATES COVERED *(From - To)*
Apr 1989	AGARD Conference Proceedings	3/1/1986 - 8/31/1986

4. TITLE AND SUBTITLE

Effects of Head Mounted Devices on Head-Neck Dynamic Response to +Gz Accelerations

5a. CONTRACT NUMBER

5b. GRANT NUMBER

5c. PROGRAM ELEMENT NUMBER

6. AUTHOR(S)

Eberhardt Privitzer, PhD
Ints Kaleps, PhD
Harry G. Armstrong

5d. PROJECT NUMBER

5e. TASK NUMBER

5f. WORK UNIT NUMBER

7. PERFORMING ORGANIZATION NAME(S) AND ADDRESS(ES)

Arvin/Calspan Corporation
P.O. Box 400, Buffalo, NY 14225
and
Aerospace Medical Research Laboratory, Biomechanical Protection Branch
Wright-Patterson Air Force Base, OH 45433-6573

8. PERFORMING ORGANIZATION REPORT NUMBER

AAMRL-TR-88-044

9. SPONSORING/MONITORING AGENCY NAME(S) AND ADDRESS(ES)

US Air Force Research Laboratory
2800 Q Street, Bldg 824
Wright-Patterson Air Force Base, OH 45433-7947

10. SPONSOR/MONITOR'S ACRONYM(S)

11. SPONSOR/MONITOR'S REPORT NUMBER(S)

12. DISTRIBUTION/AVAILABILITY STATEMENT

Approved for public release; distribution is unlimited.

13. SUPPLEMENTARY NOTES

AGARD-CP-471, Munich German, Apr 1989

14. ABSTRACT

15. SUBJECT TERMS

16. SECURITY CLASSIFICATION OF:			17. LIMITATION OF ABSTRACT	18. NUMBER OF PAGES	19a. NAME OF RESPONSIBLE PERSON
a. REPORT	b. ABSTRACT	c. THIS PAGE			John R. Buhrman
Unclassified	Unclassified	Unclassified	UU	15	19b. TELEPHONE NUMBER *(Include area code)* 937-255-3121

Privitzer, Eberhardt

"Effects of Head Mounted Devices on Head-Neck Dynamic Response to +Gz Accelerations"

Privitzer, E.

AGARD

ADVISORY GROUP FOR AEROSPACE RESEARCH & DEVELOPMENT

7 RUE ANCELLE 92200 NEUILLY SUR SEINE FRANCE

Paper Reprinted from
Conference Proceedings No.471

NECK INJURY IN ADVANCED MILITARY AIRCRAFT ENVIRONMENTS

NORTH ATLANTIC TREATY ORGANIZATION

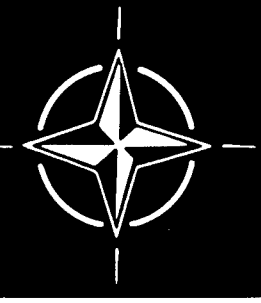

Recno 1749

EFFECTS OF HEAD MOUNTED DEVICES ON HEAD-NECK DYNAMIC RESPONSE TO $+G_Z$ ACCELERATIONS

Eberhardt Privitzer, PhD
Arvin/Calspan Corporation
P.O. Box 400
Buffalo, New York, U.S.A. 14225

and

Ints Kaleps, PhD
Harry G. Armstrong Aerospace
Medical Research Laboratory
Wright-Patterson AFB, Ohio, U.S.A. 45433-6573

SUMMARY

An investigation is described which addresses the inertial loading effects of Head Mounted Devices (HMD) on aviator head-neck-spine dynamic response during high $+G_Z$ acceleration exposure. The primary objectives of this study were to develop a methodology which could be used to establish limits on HMD inertial properties and to apply this methodology to the evaluation of the severity of the internal loads -- occurring in the neck and upper spine -- associated with certain specific HMD ensembles. This paper describes how the Head-Spine Model (HSM), a highly discretized, 3-D mathematical representation of the human head-spine-torso structure, was used to: 1) establish a set of baseline response criteria (BRC); 2) establish a preliminary methodology for setting limits on HMD inertial properties; and 3) evaluate the severity of the loading associated with possible chemical defense (CD) ensembles.

INTRODUCTION

The investigation described in this paper was part of a more encompassing program which is being conducted at the Harry G. Armstrong Aerospace Medical Research Laboratory (AAMRL) located at Wright-Patterson Air Force Base, Ohio. This program has as its overall goals the development of design guidelines for limiting the inertial properties of HMD for various dynamic environments and the establishment and implementation of methodologies that will provide accurate measurements of the inertial properties and evaluations of the inertial loading severities associated with existing or planned HMD. Motivation for this program stems from the increasing emphasis on the use of the aviator's head and/or helmet as platforms for protective and/or performance enhancement equipment such as chemical defense gear or night vision enhancement systems.

While such equipment indeed increases crewmember protection and enhances performance, organizations within the United States Air Force, Navy and Army are nonetheless concerned about the potentially adverse effects associated with HMD (1). These adverse effects arise from the c.g. (center of gravity) shifts, usually anteriorly, and increased loading, on the neck and upper spine, produced by HMD. They include excessive helmet motion relative to the head, neck muscle fatigue and, in high G environments, a potentially significant increase in the likelihood of severe injury to the neck and upper spine. Designers of HMD are endeavoring to minimize these systems' weights and c.g. distances from the head c.g. (see e.g., (2)). They are having to do so, however, without the aid of well established quantitative guidelines based on, e.g., neck and upper spine load limitations.

AAMRL's Program, which seeks to establish such quantitative guidelines, has involved both analytical and experimental aspects. The experimental work has considered the measurement of the inertial properties -- mass, inertia tensor and c.g. location -- of specific HMD, using an automated "mass properties measurement system", and the conducting of a series of $+G_Z$ impact tests on AAMRL's six inch "HYGE" vertical impact facility. The impact tests focussed on a Hybrid III manikin head-neck structure plus five specific helmet plus mask combinations, four of which represent possible CD configurations. The analytical investigation, which is emphasized in this paper, used the Head-Spine Model (HSM), a highly discretized, 3-D mathematical representation of the human head-spine-torso structure, to: 1) establish a set of baseline response criteria (BRC); 2) establish preliminary guidelines for limiting HMD inertial properties; and 3) evaluate the severity of the inertial loading associated with the five helmet plus mask configurations.

The experimental portions of AAMRL's program, along with the analytical investigation, are discussed in detail in AAMRL-TR-88-044 (3). Some aspects of this program have also been described in references (4) and (5).

MODEL DESCRIPTION

The HSM is a three-dimensional mathematical model describing the mechanical behavior, in terms of system kinematics and internal loads, of the human head-spine-torso structure. Its fully three-dimensional formulation is just one of the features which significantly distinguishes it from earlier such models. The HSM consists of two distinct components: a general purpose computer program for the dynamic analysis of three-dimensional structures; and a data base containing inertial, material, geometric and connectivity data describing the head-spine-torso structure as well as other information descriptive of the specific problem and output to be generated. The HSM has been described previously by Belytschko, et

al. (6), Belytschko and Privitzer (7), Privitzer and Belytschko (8), and Privitzer (9), thus, only a very brief description will be given here.

Figure 1 depicts mid-sagittal (X-Z) and frontal (Y-Z) plane views and also an oblique view of the initial HSM geometry. These computer graphics generated plots show only those components of the model whose local geometries are treated as constant: the head, pelvis, the vertebrae of the cervical and thoracolumbar (TL) spines and the elements of the rib cage. None of the deformable elements representing connective tissues are shown. This is actually the most complex (in terms of the number of degrees of freedom) version of the HSM and, in the interest of computational efficiency, is rarely used for studies involving large numbers of simulations.

The version of the HSM used for the study reported herein, models the neck with two parallel 3-D beam elements. One of these beam elements has nonlinear viscoelastic axial load-deformation behavior and linear viscoelastic bending behavior and is used to represent the cervical spine. The other neck beam element has only nonlinear bending behavior, i.e., it provides no resistance to purely axial deformations, and is used to account for the nonlinear stiffening effects of the soft tissue under large neck bending deformations. This element is also used to account for chin-chest contact under large neck bending deformations. The secondary loading path and nonlinear stiffening effects of the viscera-abdominal wall-diaphragm-rib cage system are accounted for with a column of nonlinear bending elements which roughly parallels the spinal column. These elements interconnect the c.g.'s of the torso segments and develop significant bending resistance only in the case of large relative rotations between adjacent segments.

The HSM's geometry is defined by the global coordinates of points identified as primary and secondary nodes and by triads of unit vectors giving the orientations of the rigid bodies. The primary nodes correspond to the c.g.s of rigid bodies and also serve as the origins of the local coordinates attached to the rigid bodies and coinciding with their principal axes of inertia. Inertial properties are specified in terms of each body's mass and principal mass moments of inertia. The secondary nodes define some local geometric features, such as vertebral geometries, and serve primarily as attachment points for the deformable elements representing the various connective tissues. The deformable elements of the HSM version employed in this study include beam elements used, e.g., to model the intervertebral discs and spring elements used, e.g., to model the spinal ligaments. Deformable element equiilibrium equations are given by:

axial forces --

$$f_{xJ} = k_x \left(\delta + \frac{2\mu_a}{\beta_a}\dot{\delta}\right), \quad f_{xI} = -f_{xJ}; \tag{1}$$

torsional moments --

$$M_{xJ} = \frac{GJ}{L}\,\theta_{xJI}, \quad M_{xI} = -M_{xJ}; \tag{2}$$

bending moments --

$$\begin{Bmatrix} M_{qI} \\ M_{qJ} \end{Bmatrix} = \frac{k_q}{1+\phi_q}\begin{bmatrix} 4+\phi_q & 2-\phi_q \\ 2-\phi_q & 4+\phi_q \end{bmatrix}\left(\begin{Bmatrix} \theta_{qI} \\ \theta_{qJ} \end{Bmatrix} + \frac{2\mu_b}{\beta_b}\begin{Bmatrix} \theta_{qI} \\ \theta_{qJ} \end{Bmatrix}\right) \tag{3}$$

and shear loads --

$$\begin{aligned} f_{yI} &= \frac{M_{zI} + M_{zJ}}{L}, \quad f_{yJ} = -f_{yI} \\ f_{zI} &= -\frac{M_{yI} + M_{yJ}}{L}, \quad f_{zJ} = -f_{zI}. \end{aligned} \tag{4}$$

All quantities in equations (1) through (4) are defined with respect to local element coordinate systems which are referred to as rigid-convected systems since they are attached to the elements and move with them through space. I and J refer to the endpoints or nodes of an element. In equation (1);

x is directed along the length of the element from node I to J,

k_x = axial stiffness (can be nonlinear),

δ = deformation,

$\dot{\delta}$ = deformation rate,

μ_a = fraction critical damping,

β_a = global axial circular frequency to be damped.

In equation (2);

G = shear modulus,
J = polar moment of inertia of the cross-sectional area,
L = element length,
θ_{xJI} = $\theta_{xJ} - \theta_{xI}$ = torsional deformation.

In equation (3);

q refers to either the y or z axes,
k_q = bending stiffness (can be nonlinear),
θ_{qI}, θ_{qJ} = bending deformations,
$\dot{\theta}_{qI}$, $\dot{\theta}_{qJ}$ = bending deformation rates,
μ_b = fraction critical damping,
β_b = global bending circular frequency to be damped,
ϕ_q = shear deformation parameter,

$$= \frac{12\, E\, I_q}{G\, A_q\, L^2}$$

E = modulus of elasticity,
I_q = second moment of the cross-sectional area about q,
A_q = area effective in shear.

Material nonlinearities are incorporated by defining k_x and k_q to be nonlinear functions of deformations.

In addition to the deformable elements representing the internal connective tissues, a system of spring elements is used to model a restraint system and viscoelastic surfaces are used to represent interaction surfaces such as an ejection seatback. The experimental and analytical bases for the selection of the HSM geometry and inertial and material properties are described in detail in references (6), (7), and (10) through (13).

The HSM computer program uses an explicit scheme for the numerical time integration of the nonlinear equations of motion for model kinematics. the approach used requires no matrix inversions. All element quantities are computed at the element level, i.e., with respect to the rigid-convected coordinates, $\hat{x}_k$. After the element by element computations have determined the element nodal loads, they are transformed and assembled into a global internal force array, F^{int} (defined in the global coordinates, X_k) and into internal moment arays, $\bar{M}_I^{int}$ (the components of which are defined with respect to the various body systems, $\bar{x}_k$), corresponding to each primary node (rigid body), I. The components of F^{int} are then used in the computations for translational kinematics via Newton's Second Law while the components of the $\bar{M}_I^{int}$ are used in the computations for rotational kinematics via Euler's Equations of Motion for each rigid body. The procedure is described in detail by Belytschko, et al.,.(14)

Spinal Injury Function and Neck Injury Parameter

The HSM has a spinal injury prediction capability, referred to as the Spinal Injury Function (SIF), which addresses the predominant ejection acceleration as well as general vertical impact acceleration induced spinal injury mode; vertebral body compressive failure resulting from combined axial compression and bending loads. It is given by:

$$SIF_V = \left\{ \left| \frac{P}{P^*} \right| + \max \left[\left| \frac{Mx}{Mx^*} \right| , \left| \frac{My}{My^*} \right| \right] \right\}_V^{max} \qquad (5)$$

where V = vertebral level of the thoracolumbar (TL) spine; P, M_x and M_y are simulation computed instantaneous equilibrium values of the compressive load and the local lateral and AP bending moments, respectively; and P*, M_x* and M_y* are the corresponding failure levels. The P* are based on rate dependent axial compression load-deformation data (to failure) (15) and (16). The corresponding data for the M_x* and M_y* were found to be insufficient. These were thus derived from the P* through the use of relationships based on assumptions on vertebral body geometry and material distribution (3). The SIF, as given by equation (5), represents the ratio of extreme fiber compressive stress to a failure or limiting value. Thus, assuming that the compressive limiting stresses are normally distributed, a value of SIF = 1 at any vertebral level V of the TL spine is taken to correspond to a 50% likelihood of vertebral body compressive failure due to combined axial compression and bending at that level.

A Neck Injury Parameter (NIP) was developed, as part of this investigation, to provide an injury prediction feature for the neck similar to the SIF for the TL spine. The NIP is given by:

$$f_N = \left\{ \left| \frac{P}{P^*} \right| + \max \left[\left| \frac{M_x^{avg}}{M^*} \right|, \left| \frac{M_y^{avg}}{M^*} \right| \right] \right\}^{max} \qquad (6)$$

where

$$M_x^{avg} = \frac{M_x^i + M_x^j}{2} \; ; \; M_y^{avg} = \frac{M_y^i + M_y^j}{2} \; ;$$

M_x and M_y refer to local lateral and A-P bending moments respectively, and the supercripts i and j refer to nodes i and j of the neck beam element and correspond to the C7-T1 and Head-C1 junctures, respectively. As is the case for the SIF, the P, M_x^{avg} and M_y^{avg} in equation (6) refer to simulation computed instantaneous equilibrium values of the compressive load and the local lateral and A-P bending moments while the P* and M* are the corresponding failure levels. Because of the approximately elliptical cross-sectional geometry of the vertebral bodies, the lateral and A-P limit bending moments for the SIF are not equal -- the lateral limit bending moments are generally larger than the A-P limit bending moments since the lateral vertebral body diameter is typically larger than the A-P diameter. For the NIP, however, it was assumed that the lateral and A-P limit bending moments are equal. Figure 2 shows the limit loads for the SIF and f_N plotted versus vertebral level (L5 through T1) for the SIF and a single point (corresponding roughly to the middle of the cervical spine) for the neck. Note that the limit loads for the neck were extrapolated from those for the TL spine.

Validation of the HSM has been pursued at AAMRL for a number of years (17). It has involved comparisons of model predictions with data obtained from experimental programs and also spinal compressive injury statistics compiled from operational ejection data. HSM dynamic response predictions have been found to compare well with data obtained from experiments with human volunteers ((7), (8), and (18)). Comparisons of HSM-SIF predictions with operational ejection injury statistics appear to be reasonable with respect to both predicted injurious acceleration profiles and spinal injury locations. Note again that the vertebral body axial compression failure levels used by the SIF, i.e., the P* in Equation (5) are based directly on data obtained from rate dependent axial compression load-deformation experiments with human vertebral bodies.

APPROACH

Our approach to the analytical study began with the use of the HSM to establish a set of limiting or baseline response criteria (BRC). These were HSM neck and spinal response predictions from a simulation with a moderate risk + G_Z half-sine acceleration exposure. Following this, HSM ejection simulations were run for different configurations of generic encumbering devices (point masses). Guidelines for setting limits on encumbrance mass and location were then established by comparing HSM neck and spinal response predictions from these simulations to the BRC. Finally, a series of HSM ejection simulations was run for the specific helmet and mask combinations considered in the experimental part of the program. The performances of these ensembles were evaluated against the HSM established guidelines.

Baseline Response Criteria

The response parameters of primary concern in this study were the NIP for the neck and the SIF for the TL spine. Thus, in order to quantify the inertial loading effects of HMD, we required a set of limiting or baseline response criteria (BRC) for these parameters. Ideally, such criteria should be based directly on appropriate experimentally measured data. For the lower TL spine, some such data do indeed exist, e.g., those on which the P* in equation (5) are based. As already mentioned, however, similar such data for the TL spine limit bending moments, M_x^* and M_y^* were insufficient. This was also true for any such data for the cervical spine. Note that what we desired for the cervical spine were limiting compression loads and bending moments at specific locations, such as specific cervical vertebrae, not limiting loads deduced from experiments with human volunteers or cadavers.

Because of this lack of appropriate experimental data, it was decided to base the BRC on the HSM's response to a moderately severe whole body + G_Z acceleration exposure. The specific profile is a 17G peak, 300 ms duration half-sine prescribed to act at the HSM pelvis c.g. and the seatback. This moderate risk exposure is based on the whole body acceleration tolerance criteria established by AAMRL for the Aerospace Medical Division's CREST (Crew Escape Systems Technologies) Program (19). The term moderate risk implies a 5% probability of spinal injury. Figure 3 shows the NIP and SIF as well as the ratios P/P* and M/M* from the HSM baseline simulation, i.e., the HSM predicted response (in terms of spinal loads) to the moderate risk $+G_Z$ half-sine exposure. Note that only one bending moment ratio is plotted for the TL spine since the response for this simulation was symmetric about the mid-sagittal (X-Z) plane. Thus the M/M* for the TL spine refer to A-P bending. The f_N and SIF given in Figure 3 are the BRC.

Ejection Simulations with Generic Encumbrances

Following the establishment of the BRC, an extensive matrix of ejection simulations was run in which generic encumbrances, i.e., point masses of 1, 2 and 3 kg, were located at 8 different points on the surface of the helmet (see Table 1). The simulations plus the nomenclature used to identify them are listed in Table 2. Note that while Tables 1 and 2

include both symmetric and asymmetric configurations, only the symmetric cases are discussed in this paper. All of the simulations, including the 17G, 300 ms half-sine exposure included the effects of a generic helmet having a mass of 1 kg, principal mass moments of inertia of 100 kg-cm^2 and with its c.g. assumed to be coincident with that of the head. The helmet was also assumed to move with the head thus its inertial properties were added directly to those of the head. Similarly, the point masses were also assumed to move with the head/helmet, thus the inertial properties of a head/helmet/point mass system were calculated with respect to the shifted c.g. of the entire system.

Table 1
COORDINATES OF POINT MASS LOCATIONS IN HEAD/HELMET LOCAL SYSTEM

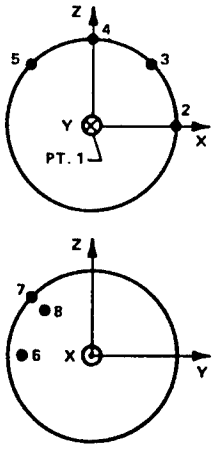

POINT MASS LOCATION	COORDINATES IN HEAD-HELMET LOCAL SYSTEM (cm) X	Y	Z
1	0	0	0
2	12	0	0
3	$12/\sqrt{2}$	0	$12/\sqrt{2}$
4	0	0	12
5	$-12/\sqrt{2}$	0	$12/\sqrt{2}$
6	$12/\sqrt{2}$	$-12/\sqrt{2}$	0
7	0	$-12/\sqrt{2}$	$12/\sqrt{2}$
8	$12/\sqrt{3}$	$-12/\sqrt{3}$	$12/\sqrt{3}$

Table 2
NOMENCLATURE FOR EJECTION SIMULATIONS WITH GENERIC ENCUMBRANCES

ID	POINT MASS LOC.	DEFINITION
BGH	–	BASELINE; GENERIC HELMET
AGH	–	ACES II; GENERIC HELMET
CG1, 2 & 3	1	1, 2 & 3 kg @ HEAD/HELMET (H/H) C.G.
A1, 2 & 3	2	1, 2 & 3 kg @ H/H ANTERIOR PT.
AS1, 2 & 3	3	1, 2 & 3 kg @ H/H ANTERIOR-SUPERIOR PT.
S1, 2 & 3	4	1, 2 & 3 kg @ H/H SUPERIOR PT.
ASPS1, 2, 3 & 4	3 & 5	0.5, 1, 1.5 & 2 kg @ H/H ANTERIOR-SUPERIOR + POSTERIOR-SUPERIOR PTS.
AR1, 2 & 3	6	1, 2 & 3 kg @ H/H ANTERIOR-RIGHT PT.
RS1, 2 & 3	7	1, 2 & 3 kg @ H/H RIGHT-SUPERIOR PT.
ARS1, 2 & 3	8	1, 2 & 3 kg @ H/H ANTERIOR-RIGHT-SUPERIOR PT.

The ejection acceleration exposure chosen for these simulations was a nominal ACES II catapult plus rocket acceleration profile with a 12 G peak and a time to peak of 140 ms (20). The 17 G, 300 ms half-sine and the ACES II acceleration profiles are plotted in Figure 4. The HSM head-neck ranges of motion are similar for both exposures. In fact, the primary criteria for the selection of the baseline exposure were 1) that it be moderate risk, 2) that it be representative of experimentally attainable exposures and 3) that it produce a head-neck range of motion similar to that associated with the nominal ACES II profile.

Figure 5 compares the HSM predicted head - neck - TL spine kinematic responses from simulations BGH, AGH and AS3 (see Table 2 for simulation nomenclature). Shown are mid-sagittal (X-Z) plane configurations at 150, 200 and 250 ms. These configurations are representative of the range of kinematic responses associated with all of the symmetric simulations. Only those components of the model whose local geometries remain constant are plotted by the HSM's plotting software. Thus, in this case, the head or the head/helmet/encumbrance system, the pelvis and the vertebrae of the TL spine are plotted while the deformable elements of the TL spine and the neck beams are not. A reasonable estimate of the deformed geometry of the beam element representing the cervical spine can, however, be obtained from the kinematics of the head (or head/helmet/encumbrance system) and T1 -- hence the dashed curve approximating the deformed geometry of this element in the 200 ms configurations. Kinematically speaking (and also qualitatively), it is quite apparent that the AGH response is less severe than the BGH response, while the AS3 response is more severe. Figure 6 compares head mid-sagittal plane rotations from simulations BGH, AGH and AS3 while Figure 7 compares T1 rotation time histories. The BGH and AGH responses are quite similar except for the higher magnitude of the BGH head and T1 rotations resulting from the higher peak acceleration of the 17G, 300 ms half-sine exposure.

Ejection Simulations with Specific HMD

Following the completion of the HSM ejection simulations with the generic HMD, additional ejection simulations were run which incorporated five specific helmet plus mask combinations used in the experimental portion of this program. Two helmets were considered; a "pilot's" helmet (HGU-55/P) and a "flyer's" helmet (HGU-39/P). Three masks were considered: a pilot/crewmember oxygen mask (MBU-12/P) and two chemical-biological-oxygen (CBO) masks (MBU-13/P and AR-5). The inertial properties of the helmet plus mask configurations were obtained in the experimental portion of the program.

Table 3 lists the five specific helmet plus mask combinations and the inertial properties of the complete helmet + mask + head systems. These data are also included for the generic encumbrance configurations for simulations AGH, CG1, CG2 and CG3 for comparison purposes. Since the simulations were symmetric with respect to the mid-sagittal (X-Z) plane -- as were the inertial properties (at least nearly so) of the specific HMD -- the relevant inertial properties are mass, principal mass moment of inertia about the lateral axis through the system c.g. (I_y), and the X and Z locations of the system c.g. with respect to the unencumbered head c.g. The HSM unencumbered head has a mass of 4.38 kg and an I_y of 233.0 kg-cm^2 compared to 4.54 kg and 240.0 kg-cm^2, respectively, for the Hybrid III head. The parameters R_N and R_S(T1) will be described in the next section.

Table 3
SPECIFIC HMD CONFIGURATIONS, INERTIAL PROPERTIES, AND R_N (NIP RATIOS) AND R_S (T1) (SIF(T1) RATIOS) FROM SIMULATIONS WITH SPECIFIC HMD

CONFIGURATION	HELMET	MASK OR POINT MASS	SYSTEM[1] MASS (kg)	SYSTEM[1] I_y (kg-cm²)	SYSTEM C.G. LOCATION (cm)[1] x	z	R_N	R_S (T1)
1	HGU-55/P	MBU-12/P[2]	5.75	383.	-0.43	-0.34	0.91	0.61
2	HGU-55/P	MBU-13/P[3]	6.11	424.	-0.16	-0.27	0.90	0.67
3	HGU-55/P	AR-5[3]	6.19	486.	-0.60	-1.18	0.90	0.65
4	HGU-39/P	MBU-13/P	6.60	513.	-0.38	-0.63	0.95	0.70
5	HGU-39/P	AR-5	6.68	499.	-0.76	-0.94	0.99	0.66
AGH	"Generic"	—	5.38	333.	0.0	0.0	0.84	0.59
CG1	"Generic"	1.0	6.38	333.	0.0	0.0	0.93	0.71
CG2	"Generic"	2.0	7.38	333.	0.0	0.0	1.0	0.82
CG3	"Generic"	3.0	8.38	333.	0.0	0.0	1.02	0.94

NOTES:
(1) helmet + mask + head
(2) oxygen mask
(3) chemical-biological-oxygen (CBO) mask

RESULTS

The inertial loading effects of first the generic encumbering devices and then the specific HMD were evaluated by comparing the HSM NIP and SIF predictions, from the ejection simulations with those devices, to the BRC, i.e., the NIP and SIF predictions from the simulation with the 17G, 300 ms half-sine exposure (simulation BGH - Baseline with Generic Helmet). These comparisons were accomplished by dividing the NIP and SIF from the ejection simulations by the corresponding BRC values and then plotting these ratios versus spinal level. Thus when any of these ratios exceed 1.0, the corresponding BRC or limiting value is exceeded.

Results from Ejection Simulations with Generic HMD

Figures 8 and 9 show the effects of varying a point mass from 0 to 3 kg at locations 2 and 3, the head/generic helmet anterior and anterior - superior points, respectively. Figure 10 shows the NIP and SIF ratios as functions of the location of a 2 kg point mass - actually case 5 corresponds to a 1 kg point mass located at both sites 3 and 5. Results are plotted for the neck and vertebral levels T1 through T6. The lower levels (T7 through L5) are not included because the inertial loading effects of the point masses were found to decrease with increasingly lower vertebral level. It was also found that, for all cases of interest, the largest ratios involved the NIP and SIF(T1) (SIF at T1). This observation indicates that we actually do not need to consider 18 BRC (the 17 SIF plus the NIP). Rather, we can focus on two parameters in particular: the SIF ratio at T1, which for convenience will be referred to as R_S(T1); and the NIP ratio, which will be referred to as R_N, i.e.,

$$R_S(T1) = \frac{SIF(T1)}{BRC\ SIF(T1)} \tag{7}$$

and

$$R_N = \frac{f_N}{BRC\ f_N} \tag{8}$$

These two parameters are plotted in Figure 11 for all of the ejection simulations with the symmetrically located (with respect to the X-Z plane) point masses. The point mass locations are arranged in order of increasing distance forward from the head c.g. or, for locations 3 plus 5 and 4, in the order of increasing radial distance. One conclusion which can immediately be drawn from this Figure is that the inertial loading effects of HMD become increasingly more severe with increasing distance of the HMD c.g. forward from the head c.g.

The results plotted in Figure 11 appear to be ideally suited for interpretation in a pass/fail sense. Thus if the pass criteria are taken to be both R_N and R_S(T1) ≤ 1.0, the

cases which pass are AGH (generic helmet only), CG1 and 2, ASPS1 and S1. None of the cases considered at locations 2 and 3, which are common attachment sites for HMD such as CBO masks, night vision imaging systems and visors, pass. Note that all of the simulations included the effects of a 1 kg generic helmet with I_y = 100 kg-cm^2. Thus, according to Figure 11, the upper bound on the mass of a head mounted ensemble (i.e., helmet + mask + additional HMD) is 3 kg, provided the c.g. of the ensemble is coincident with that of the head and I_y of the ensemble does not exceed 100 kg-cm^2. It is unlikely that I_y of a 3 kg mass HMD ensemble would be less than 100 kg-cm^2 -- a relatively light helmet plus mask combination, such as the HGU-55/P plus the MBU-12/P, which weighs approximately 1.4 kg, has an I_y in excess of 100 kg-cm^2. Thus the maximum allowable mass for an HMD ensemble with c.g. coincident with the head c.g. appears to be less than 3 kg and the maximum allowable HMD mass above the 1 kg generic helmet appears to be less than 2 kg.

The HMD mass limit decreases with increasing distance from the head c.g. (particularly anteriorly). For an HMD with c.g. at location 3 and with a "counterweight" at location 5, the mass limit as indicated in Figure 11 is approximately 1.1 - 0.55 = 0.55 kg. The "counterweight" mass is subtracted off since it is merely a dead weight added to the ensemble to reduce the potential for neck muscle fatigue. It has nothing to do with the actual operation of the HMD. For location 4, the HMD mass limit appears to be approximately 1 kg; and for locations 3 and 2, approximately 0.6 kg.

When one considers that a typical helmet plus mask ensemble -- worn in the high speed, fixed-wing aircraft operational environment, which, in an emergency, can require crewmember ejection -- can weigh approximately 2 kg, the HMD mass limits indicated in Figure 11 appear to be somewhat conservative. A likely source for this conservatism comes from the following. The half-sine acceleration profile used to establish the BRC was identified as a moderate risk exposure. It should be emphasized, however, that it is a moderate risk exposure for the lower thoracic and lumbar spines. Based on AAMRL compilations of ejection acceleration induced spinal injury statistics, the likelihood of cervical spine vertebral body compressive fractures during ejection acceleration exposure appears to be significantly lower than the likelihood of vertebral body compressive fractures in the lower thoracic and lumber spines. Thus, while the BRC for the lower thoracic and lumbar spines may indeed represent moderate risk criteria, the BRC used in generating Figure 11, i.e., the BRC f_N and SIF(T1) could very well represent low risk criteria. Since our goal was to establish guidelines based on moderate risk criteria, the results given in Figure 11 are probably conservative.

Analytical Evaluation of Specific HMD

The inertial loading effects of five helmet plus mask combinations were evaluated by comparing the R_N and R_S(T1) computed for the ejection simulations with those ensembles to the preliminary guidelines contained in Figure 11. The first combination, HGU-55/P + MBU-12/P, represents a standard pilot's configuration. The remaining four combinations; HGU-55/P + MBU-13/P, HGU-55/P + AR-5, HGU-39/P + MBU-13/P, and HGU-39/P + AR-5, represent four possible CD configurations.

The R_N and R_S(T1) for the ejection simulations with the specific HMD are listed in Table 3 along with the same parameters for simulations AGH, CG1, CG2 and CG3. All the R_N and R_S(T1) for the specific HMD configurations are less than 1.0. Thus all of these configurations pass the criteria that both R_N and R_S(T1) be $\leq$1.0. While the R_N and R_S(T1) appear to vary nearly linearly with mass for the generic HMD, their variations with mass and I_y of the specific HMD configurations are considerably less linear. This occurs because, while the c.g. for the generic HMD at location 1 (the head c.g.) is constant, the c.g.s for the specific HMD vary as indicated in Table 3. It is quite evident from Figure 11, that HMD c.g. location can be as significant with regards to HMD inertial loading effects as mass or moment of inertia.

CONCLUSIONS

The following are the main findings of the analytical investigation.

1. The inertial loading effects of HMD are observable in the internal loads developed in the neck and throughout the TL spine with the severity of these effects increasing with increasing (towards the head) spinal level.

2. Two parameters particularly useful in evaluating the inertial loading effects of HMD are R_N, the ratio of the computed neck injury parameter (NIP) to the baseline response criteria (BRC) NIP; and R_S(T1), the ratio of the computed SIF(T1) to the BRC SIF(T1).

3. The results contained in Figure 11 represent preliminary guidelines for limiting HMD mass and location with respect to the head c.g. for the purpose of minimizing the inertial loading effects of such devices during ejection acceleration exposures. The HMD pass criteria contained in these guidelines are R_N and R_S(T1)$\leq$ 1.0. These criteria appear to be conservative when viewed as moderate risk (5% probability of injury) criteria.

4. The inertial loading effects of HMD become increasingly more severe as they are located increasingly further, particularly anteriorly, from the head c.g.

5. All of the specific HMD ensembles -- helmet + mask combinations -- considered satisfy the pass criteria, R_N and R_S(T1)$\leq$1.0.

6. For the four CD configurations: the two involving the HGU-55/P helmet are less severe in terms of their inertial loading effects than the two involving the HGU 39/P.

The flexible rubber shroud of the AR-5 posed significant difficulties during the inertial properties measurements. The shroud had to be rolled/folded together and lumped at the base of the helmet so that the measurement procedure could be executed. As the shroud is actually at least partially draped over the air person's shoulders, the coupling of the entire shroud to the base of the helmet most likely compromised our measurements. Since these data were used directly for the HSM simulations, we feel that it is not appropriate to use the results listed in Table 3 to quantitatively compare the inertial loading effects of the AR-5 and MBU-13/P CBO masks.

The analytical investigation described in this paper and the related experimental work discussed in (3) and (5), have demonstrated analytical and experimental methodologies required to 1) establish general HMD design guidelines, and 2) define the inertial properties and evaluate the inertial loading effects of specific existing and planned HMD ensembles. This effort also produced some HMD design guidelines for ejection acceleration exposures. Based on the results obtained and the experience gained from this program, we have defined further analytical and experimental investigations designed to produce 1) general HMD design guidelines for various acceleration environments in the form of, e.g., spatial envelopes of HMD mass limits versus the coordinates of HMD c.g.s, and 2) accurate measurements of the inertial properties and evaluations of the inertial loading severities associated with specific existing or planned HMD ensembles.

REFERENCES

1. Helmet Standardization Working Group Meeting, Wright-Patterson AFB, OH, 14-15 August 1986.

2. "Folded Optics Create Thin, See-Through Night Vision Systems", Design News, pp. 92-93, November 3, 1986.

3. Privitzer, E., Settecerri, J.J. and Kaleps, I., "Inertial Loading Effects of Head Mounted Systems", Harry G. Armstrong Aerospace Medical Research Laboratory Tech Report, AAMRL-TR-88-044, Wright-Pattersen AFB, OH, cleared for publication.

4. Privitzer, E. and Settecerri, J.J., "Dynamic Analysis of Inertial Loading Effects of Head Mounted Systems", SAFE Journal, V. 17, No. 2, pp. 16-22, 1987.

5. Settecerri, J.J., McKenzie, J., Privitzer, E. and Beecher, R.M., "Mass Properties and Inertial Loading Effects of Head Encumbering Devices", Proc. 25th Annual SAFE Symposium, Las Vegas, NV, November 1987.

6. Belytschko, T., Schwer, L. and Schultz, A., "A Model for Analytic Investigation of Three Dimensional Spine-Head Dynamics", AMRL-TR-76-10, Aerospace Medical Research Laboratory, WPAFB, OH, April 1976.

7. Belytschko, T. and Privitzer, E., "Refinement and Validation of a Three Dimensional Head-Spine Model", AMRL-TR-78-7, Aerospace Medical Research Laboratory, WPAFB, OH, Aug. 1978.

8. Privitzer, E. and Belytschko, T., "Impedance of a Three-Dimensional Head-Spine Model", J. Mathematical Modeling 1, No. 2 pp. 189-209, 1980.

9. Privitzer, E., "Model Evaluation of Spinal Injury Likelihood for Various Ejection System Parameter Variations", 55th Shock and Vibration Bulletin, 1985.

10. Mohr, G.C., Brinkley, J.W., Kazarian, L.E. and Millard, W.W., "Variations of Spinal Alignment in Egress Systems and Their Effect", J. Aerospace Medicine 40, No. 9, pp. 983-988, September 1969.

11. Liu, Y.K. and Wickstrom, J.K., "Estimation of the Inertial Property Distribution of the Human Torso from Segmented Cadaveric Data", Perspectives in Biomedical Engr., 1973.

12. Schultz, A., Belytschko, T. and Andriacchi, T., "Analog Studies of Forces in the Human Spine: Mechanical Properties and Motion Segment Behavior", J. Biomechanics 6, pp. 373-383, 1973.

13. Schultz, A., Benson D. and Hirsch, C., "Force-Deformation Properties of Human Costo-Sternal and Costo-Vertebral Articulations", J. Biomechanics 7, pp. 311-318, 1974.

14. Belytschko, T., Schwer, L. and Klein, M.J., "Large Displacement, Transient Analysis of Space Frames", Int'l. J. Num. Methods in Engr. 11, pp. 65-84, 1977.

15. Payne, P.R., "Some Aspects of Biodynamic Modeling for Aircraft Escape Systems", Proc. Symposium on Biodynamic Models and Applications, AMRL-TR-71-29, pp. 233-335, Aerospace Medical Research Laboratory, WPAFB, OH, Dec. 1971.

16. Kazarian, L. and Graves, G.A., "Compressive Strength Characteristics of the Human Vertebral Centrum", Spine 2, No. 1, March 1977.

17. Privitzer, E., Hosey, R. and Ryerson, J., "Validation of a Biodynamic Injury Prediction Model of the Head-Spine System", Proc. AGARD AMP Specialists Mtg., Cologne, Federal Republic of Germany, April 1982.

18. Belytschko, T., Rencis, M. and Williams, J., "Head-Spine Structure Modeling: Enhancement to Secondary Loading Path Model and Validation of Head-Cervical Spine Model", AAMRL-TR-85-019, AF Harry G. Armstrong Aerospace Medical Research Laboratory, WPAFB, OH, July 1985.

19. Brinkley, J.W., "Acceleration Exposure Limits for Escape System Advanced Development", SAFE Journal, Vol. 15, No. 2, 1985.

20. "ACES II: Advanced Concept Ejection Seat", Report MDC J4576 Revision C, McDonnell Douglas Corporation, 1983.

Acknowledgement. Catherine Swigonski's excellent composition of this paper is greatly appreciated.

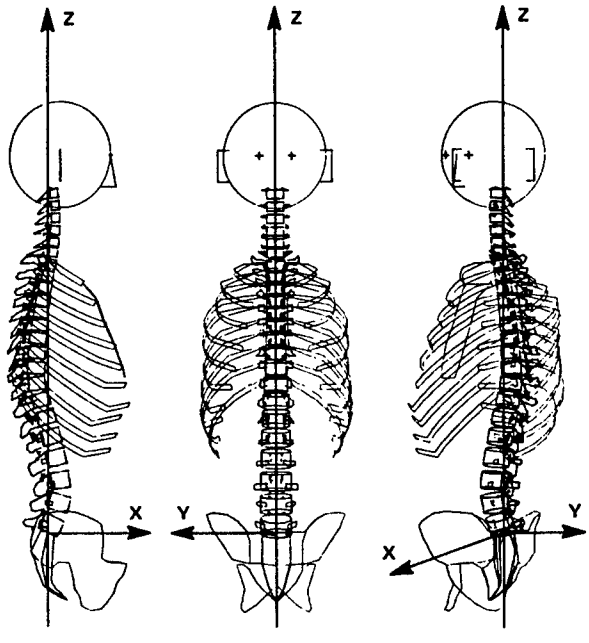

Figure 1. MID-SAGITTAL (X, Z), FRONTAL (Y, Z) AND OBLIQUE VIEWS OF HSM GEOMETRY

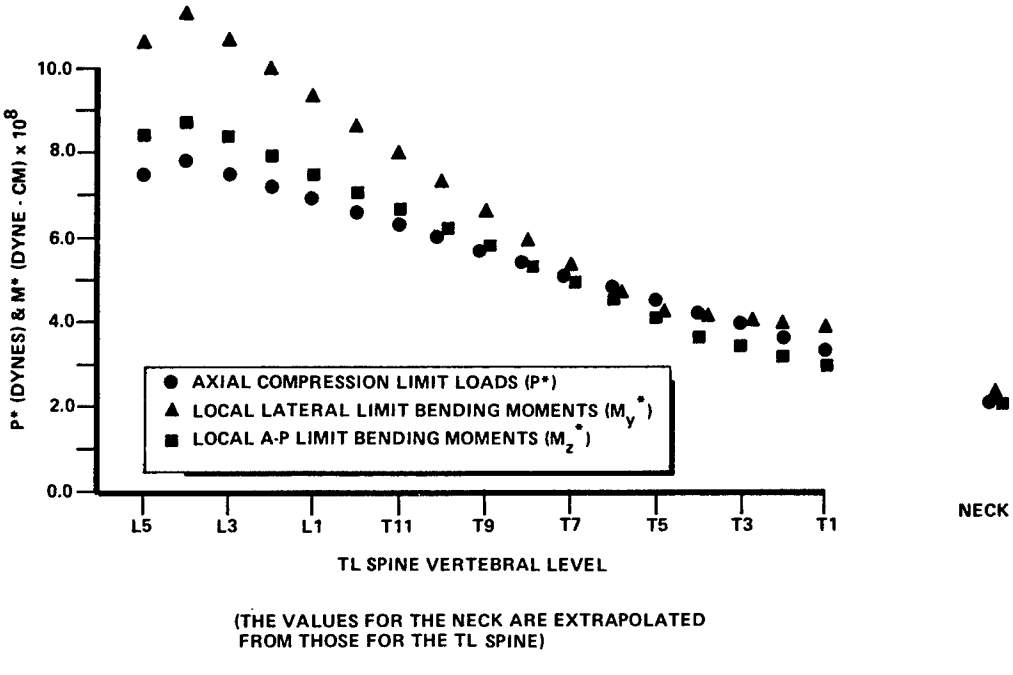

Figure 2 LIMIT LOAD DISTRIBUTION FOR THE TL SPINE (NECK VALUES ARE EXTRAPOLATED FROM THOSE FOR THE TL SPINE)

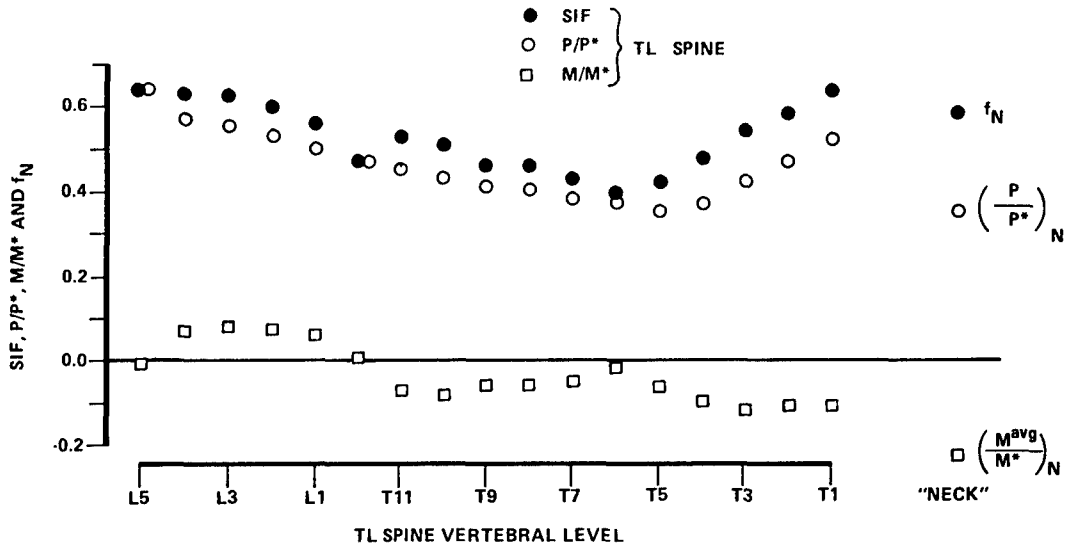

Figure 3 SIF, P/P*, M/M* AND f_N FROM BASELINE SIMULATION-
FILLED IN CIRCLES ARE BRC

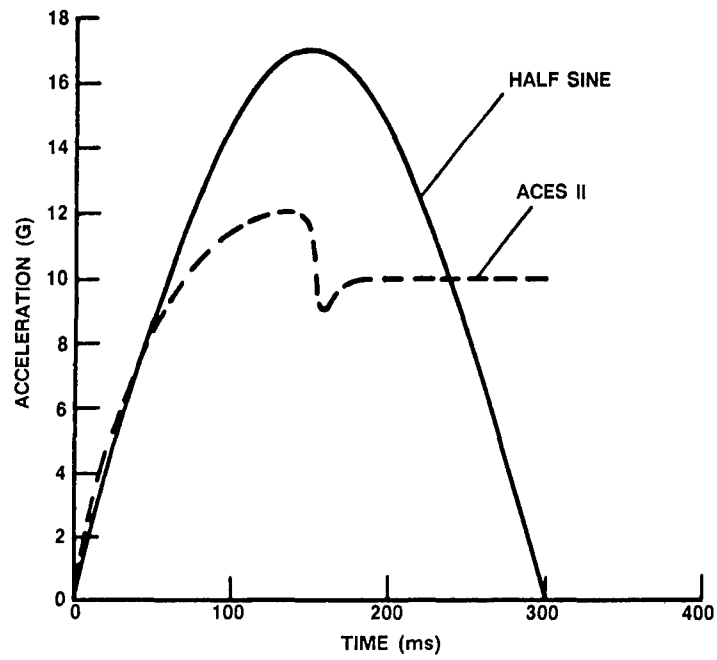

Figure 4 17G PEAK,300 ms HALF-SINE AND NONIMAL ACES II
CATAPULT PLUS ROCKET ACCELERATION PROFILES

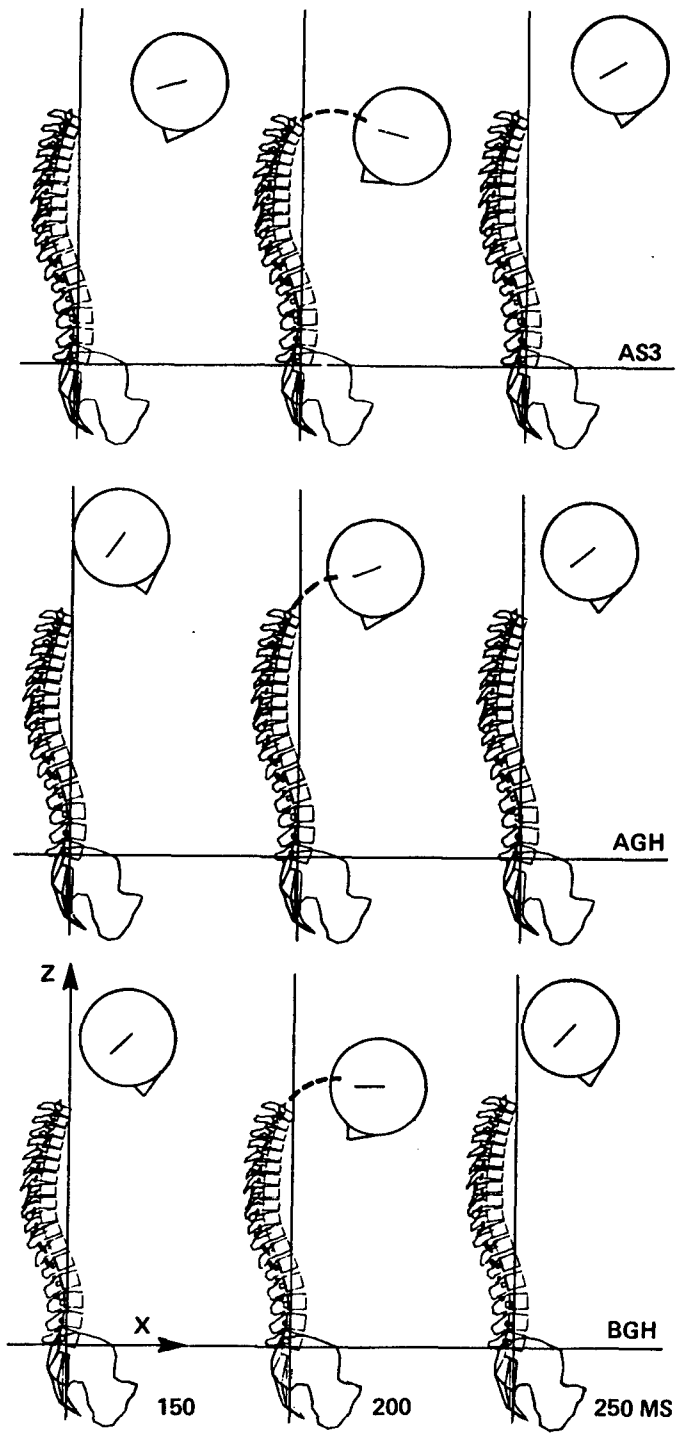

Figure 5 HSM MID-SAGITTAL (X,Z) PLANE CONFIGURATIONS AT 150, 200 AND 250 MS FOR SIMULATIONS BGH, AGH AND AS3

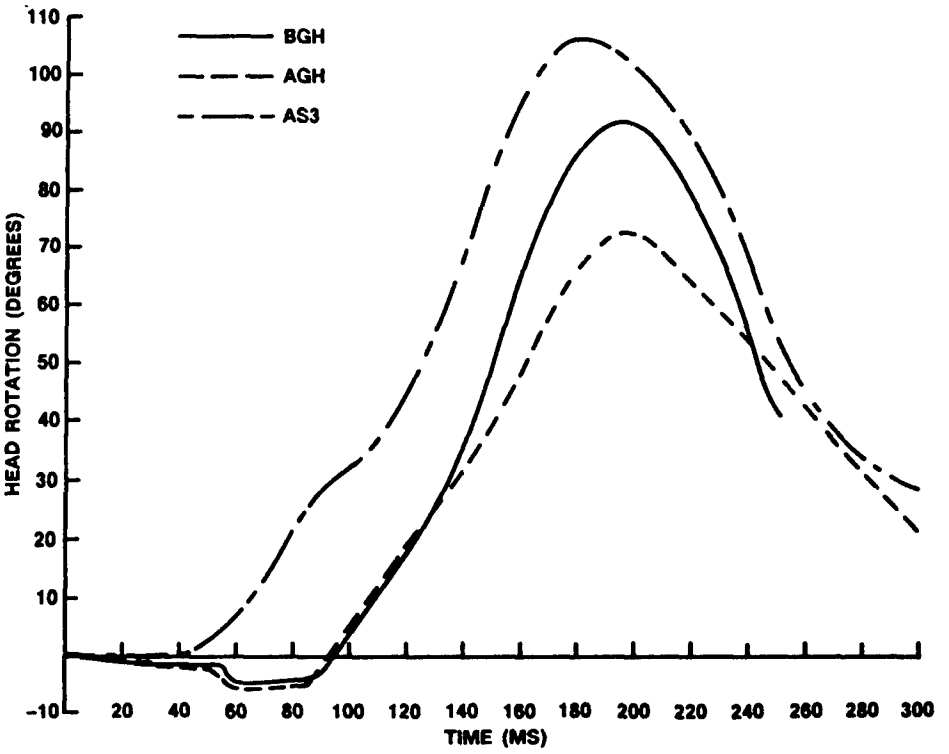

Figure 6 MID-SAGITTAL (XZ) PLANE HEAD ROTATIONS FROM SIMULATIONS BGH, AGH AND AS3

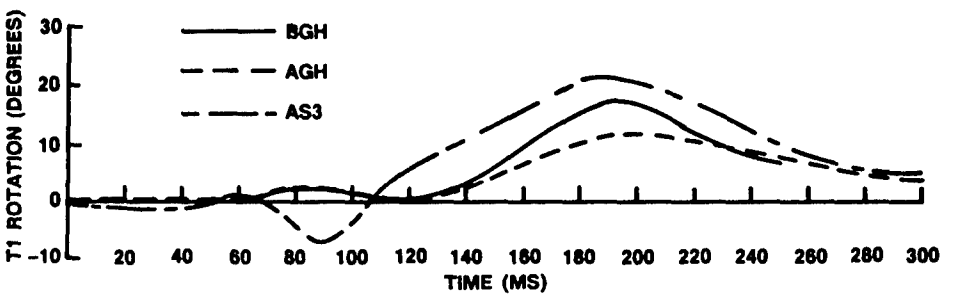

Figure 7 MID-SAGITTAL (XZ) PLANE T1 ROTATIONS FROM SIMULATIONS BGH, AGH AND AS3

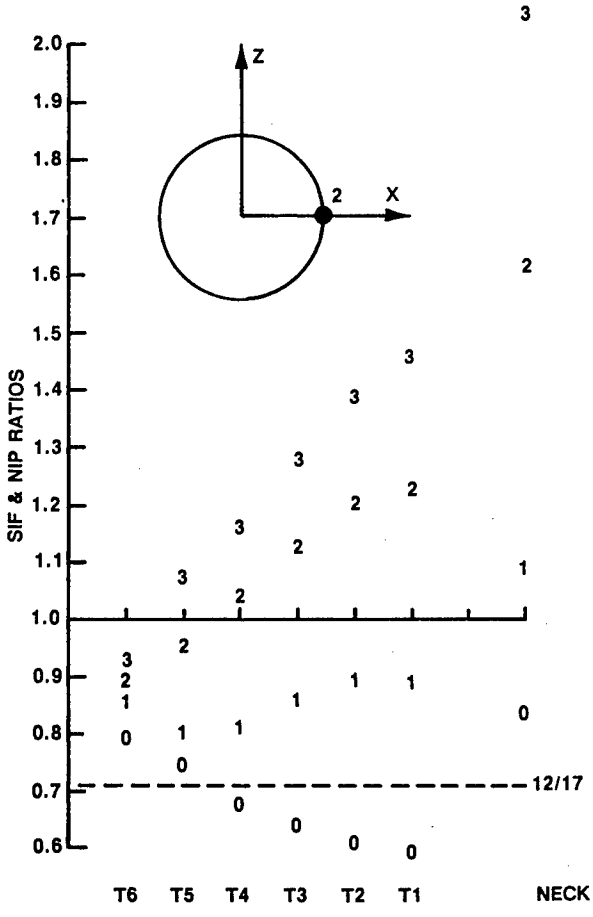

Figure 8 SIF RATIOS AND NIP RATIO FOR SIMULATIONS AGH, A1, A2 AND A3: 0, 1, 2 AND 3KG POINT MASSES AT LOCATION 2, THE ANTERIOR POINT

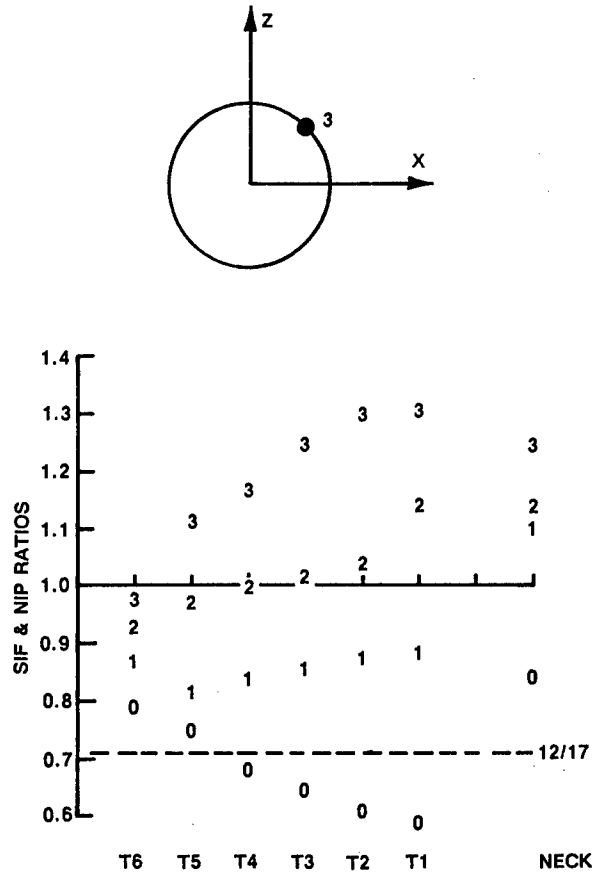

Figure 9 SIF RATIOS AND NIP RATIO FOR SIMULATIONS AGH, AS1, AS2 AND AS3: 0, 1, 2 AND 3KG POINT MASSES AT LOCATION 3, THE ANTERIOR-SUPERIOR POINT

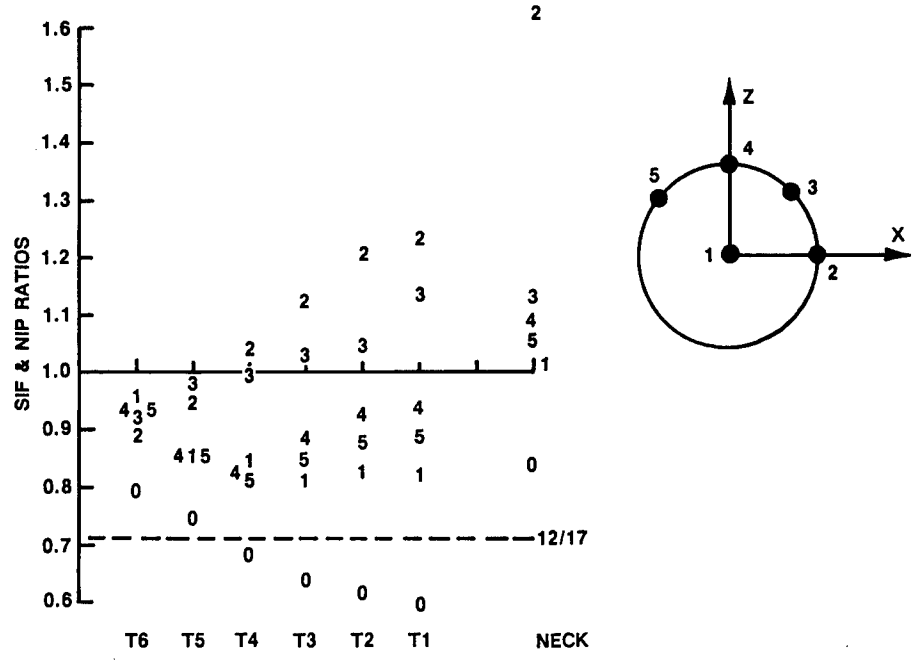

Figure 10 SIF RATIOS AND NIP RATIO VERSUS LOCATION OF 2KG POINT MASS

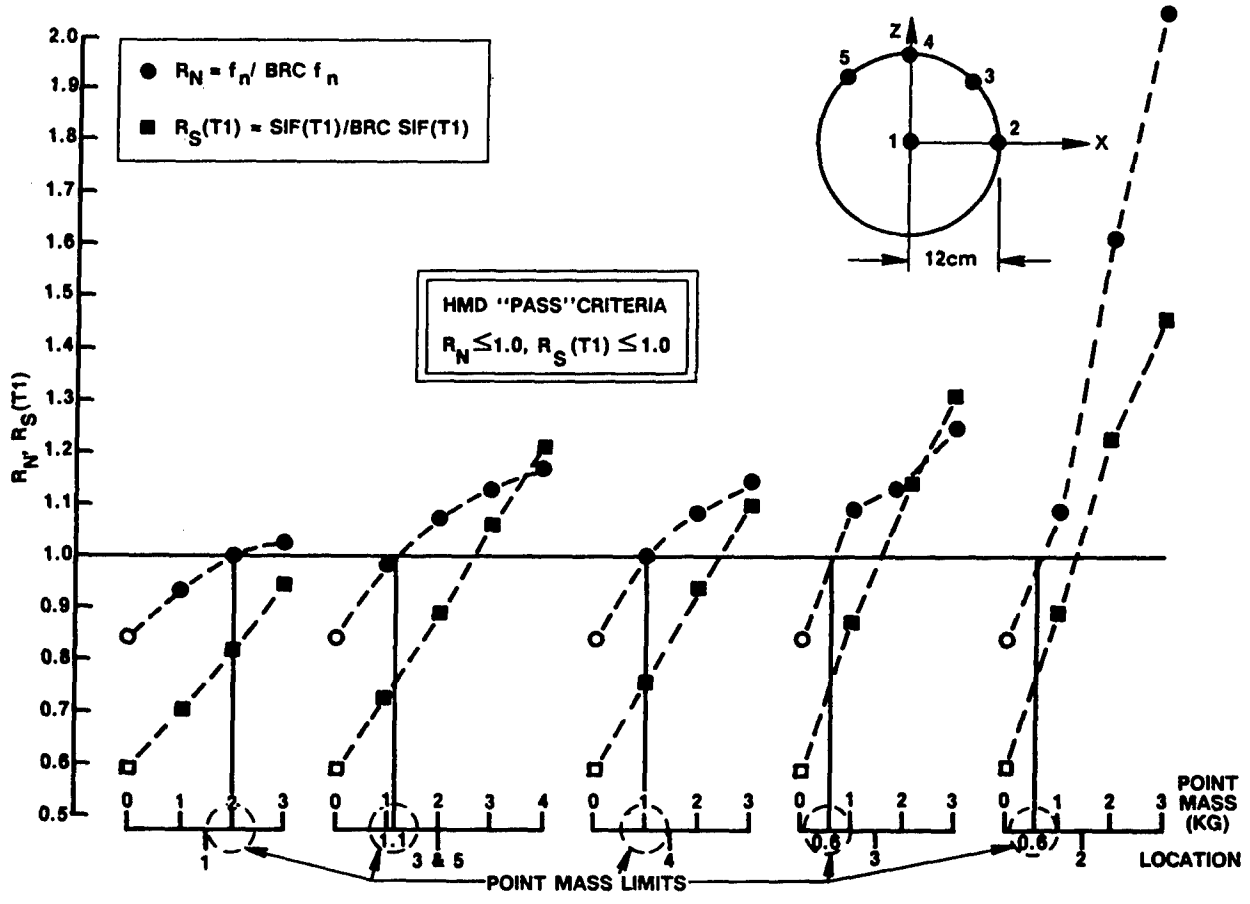

Figure 11 R_N AND R_S(T1) FOR ALL HSM EJECTION SIMULATIONS WITH SYMMETRICALLY LOCATED POINT MASS: POINT MASS LIMITS